Transport Phenomena and Kinetics in an Extravascular Bioartificial Pancreas

Bora M. Buladi, Chen C. Chang, Joanne M. Belovich, and Jorge E. Gatica
Dept. of Chemical Engineering, Cleveland State University, Cleveland, OH 44115

A bioartificial pancreas, consisting of immobilized islets encapsulated within hollow fibers, is investigated as an alternative treatment for insulin-dependent diabetes. A mathematical model is developed to determine whether this configuration of the bioartificial pancreas can yield an insulin response to a glucose challenge with the appropriate dynamics in diabetic humans. The model consists of the 2-D mass-conservation equations for glucose and insulin within the hollow fiber and capillaries. The equations contain terms for insulin-production kinetics by porcine islets and glucose-consumption kinetics. The boundary conditions account for transport resistances of the fiber membrane, the tissue surrounding the implant, and a thin film within the capillaries. The equations are coupled to a pharmacokinetic model of the circulatory system. The calculations show that an optimized design with this configuration will be feasible for human use and requires a total volume of 4.6 mL to reach the target insulin concentration in the bloodstream following a glucose challenge. The parameters and processes controlling the system performance are discussed.

Introduction

The transplant of immunoisolated islets is a promising treatment for insulin-dependent diabetes mellitus (IDDM) (Clayton et al., 1993; Mikos et al., 1994; Reach, 1993). This approach is based on the observation that islet tissue secretes insulin in response to an increase in glucose concentration. The islets are enclosed within semipermeable membranes that permit the passage of glucose and insulin, but are impermeable to larger molecules such as antibodies and lymphocytes, thereby preventing immunorejection. Since the cells are immunoisolated from the host, the transplant of islets from nonhuman species to humans may be possible. Rat (Lacy et al., 1991; Lim and Sun, 1980) and porcine islets (Inoue et al., 1992; Sun et al., 1993) have proven to behave similarly to human islets (Warnock et al., 1988) by secreting insulin in response to an increase in glucose concentration near the cells. Porcine insulin is very similar to human insulin, and the supply of pancreata from slaughtered pigs is plentiful and inexpensive, leading porcine islets to be the most likely source of tissue for transplant to humans.

A number of techniques for encapsulating and implanting islets exist. These techniques can be divided into two general classifications: those implants that are grafted to a blood vessel (intravascular devices), and those implanted directly into the tissue (extravascular devices). The intravascular devices commonly involve a shell and tube configuration, with the cells located in the annular space between two concentric hollow fibers. The inner fiber is grafted to a blood vessel, while the outer fiber precludes any contact between the islets and the patient's tissue (Jaffrin et al., 1988; Sullivan et al., 1991; Ramirez et al., 1992). This method has the advantage that blood flow through the inner fiber facilitates transport of glucose, oxygen, and insulin. Consequently, a fast response of insulin secretion to a glucose challenge, which is necessary for efficient glucose control, is ensured. The disadvantages of this device are associated with the vascular graft. The contact of blood with polymer surfaces tends to cause thrombosis, which can occlude the artery. Furthermore, since the implant must be surgically grafted, potential health risks for the patient from graft failure, or infection resulting from the insertion procedure, may be incurred.

Extravascular devices, on the other hand, pose fewer risks to the patient compared to the technique just described. A common design of an extravascular device is the encapsula-

Correspondence concerning this article should be addressed to J. M. Belovich.

tion of islets in alginate-poly-1-lysine spheres. Encapsulated islets from dogs, pigs, and rats have maintained normoglycemia in diabetic mice and rats for several months (Calafiore et al., 1990; Darquy et al., 1990; Fan et al., 1990; Fritschy et al., 1991; Krestow et al., 1991; Lim and Sun, 1980; Sun et al., 1993; Weber et al., 1990). These capsules were implanted in tissue, without direct attachment to any blood vessel.

An alternative to alginate-poly-1-lysine spheres is the encapsulation of islets into end-sealed hollow fibers (Altman, 1988, 1992; Lacy et al., 1991; Lanza et al., 1991; Penfornis et al., 1990; Ward, 1993; Zekorn et al., 1990). This configuration provides the advantage that the removal of several long, thin fibers from the patient will be easier to accomplish than the removal of thousands of microcapsules. The islets may be immobilized in alginate prior to encapsulation by the membrane, in order to keep the islets uniformly distributed throughout the fiber.

Extravascular designs have the advantage that the risks associated with the implant are minimal since no vascular graft is performed and blood flow does not directly contact the membrane surface. The primary disadvantage of this system is the distance between the cells and the blood supply, which may result in a slow insulin response. This effect may become accentuated with time as cells and proteins accumulate on the surface of the fiber, further increasing mass-transfer limitations. This problem has been circumvented by several new membrane designs (Ward et al., 1993; Sarver et al., 1995). Not only was the fibrotic reaction lacking from these implanted membranes, but vascularization of the membrane had been observed. Vascularization can be expected to cause the transport resistances to diminish, resulting in faster response of the implant to a glucose challenge.

Despite the potential for mass-transfer limitations, experimental studies of extravascular devices have proven successful in animals, as described in the literature referenced earlier. However, substantial investigations of the transport mechanisms should be performed before the devices are tested in humans. A mathematical model of the system permits one to quantify the effect of design parameters on performance indicators, such as insulin response time, insulin concentration in the blood, and the size of the device needed for human use. This information can then be used in deciding whether this approach to diabetes treatment in humans is feasible.

Mathematical models of several designs of the bioartificial pancreas have been developed (Jaffrin et al., 1988; Kelsey et al., 1990; Pillarella and Zydney, 1990a,b; Reach and Jaffrin, 1990; Sarver and Fournier, 1990). These models, however, have focused on the intravascular-style devices, which rely primarily on convective rather than diffusive transport. Moreover, these models are based on rat, rather than porcine, insulin secretion kinetics. A mathematical model has been derived for an extravascular device consisting of a chamber containing islets, adjacent to a vascularized support structure (Fournier, 1995; Sarver et al., 1995). The model is based on the pharmacokinetic approach where unsteady-state mass balances are written for each of four compartments: the implant chamber, the matrix-tissue region, the matrix capillaries, and the blood-distribution volume. This approach assumes that each compartment is well mixed. Transport resistances between compartments are accounted for using permeability coefficients.

The mathematical model presented in this article was developed in order to investigate in detail the transport characteristics and feasibility of an extravascular device consisting of end-sealed hollow fibers. The model consists of transient mass conservation equations for glucose and insulin within the hollow fiber and in the capillaries surrounding the fiber, accounting for radial and axial mass-transport and insulin-secretion mechanisms. The insulin-secretion kinetic parameters are obtained from insulin-secretion data of porcine islets (Inoue et al., 1992), using a model formulated in the literature (Pillarella, 1989). The solution of these equations provides insulin and glucose concentration profiles within the hollow fiber. These equations are coupled to a pharmacokinetic model of the human circulatory system for predicting the dynamics of insulin concentration in the bloodstream. Design parameters include number of islets to be placed in the fiber, membrane permeability, fiber length, fiber diameter, blood velocity, and implantation site.

Model Formulation

The bioartificial pancreas, as it would appear after implantation in the body, is shown in Figure 1. The hollow fiber contains islets immobilized in alginate, the ends of the fiber are sealed, and the fiber is surrounded by tissue containing a random arrangement of capillaries. Insulin, glucose, oxygen, and other nutrients and waste products, diffuse between the capillaries and the islets; the resistances to transport of these molecules include the capillary walls, tissue, the fiber membrane, the alginate, and the cell membrane. Collagen and fibroblasts may adsorb to the surface of the fiber providing, in turn, additional diffusional resistances.

Given the complex nature of the implanted bioartificial pancreas, a number of approximations are made in the development of the mathematical model. For the sake of simplifying the mathematical description, the insulin and glucose transport in the tissue surrounding the fiber are lumped radially. The concentric ring of tissue and capillaries surrounding the fiber is therefore lumped into a one-dimensional transport equation, where insulin and glucose concentrations change along the axis of the fiber only. The one-dimensional

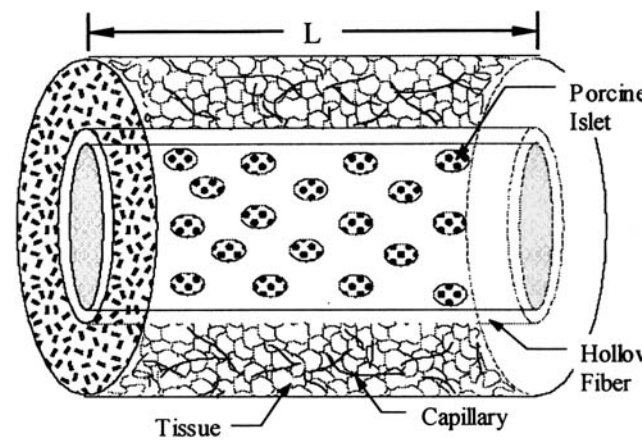

Figure 1. Single fiber containing islets, implanted in tissue.

equations will yield a single concentration value in the surrounding tissue. Details on the lumped-resistance formulation and physical significance of the variables are presented in the Appendix.

The islet distribution within the alginate is assumed to be homogeneous and isotropic. Also, insulin secretion and glucose consumption are assumed to be a continuous function of space, even though the islets, which are the sites of insulin secretion, are discretely distributed. Since the data used in the derivation of the kinetic parameters include the processes of both insulin production by the cells within the islet and the transport across the cell membrane, the mechanism of insulin transport across the cell membrane is not considered separately.

The model consists of three compartments. The first compartment consists of glucose and insulin diffusion and kinetics within the hollow fiber. The second compartment consists of convective and diffusive insulin and glucose transport in the capillary. These two compartments are coupled via boundary conditions that represent insulin and glucose transport between the hollow fiber and the blood. The third part consists of an overall insulin balance in the circulatory system.

Transport phenomena in the fiber

The conservation equations for glucose and insulin are

$$D_{G-a}\left[\frac{1}{r}\frac{\partial}{\partial r}\left(r\frac{\partial C_G}{\partial r}\right)+\frac{\partial^2 C_G}{\partial z^2}\right]-R_G(C_G)=\frac{\partial C_G}{\partial t} \quad (1)$$

$$D_{I-a}\left[\frac{1}{r}\frac{\partial}{\partial r}\left(r\frac{\partial C_I}{\partial r}\right)+\frac{\partial^2 C_I}{\partial z^2}\right]+R_I(C_G(t,r),t)=\frac{\partial C_I}{\partial t}, \quad (2)$$

where C_G is the glucose concentration in the alginate within the hollow fiber, C_I is the insulin concentration in the alginate within the hollow fiber, D_{G-a} and D_{I-a} are the effective diffusion coefficients of glucose and insulin through alginate, and $R_G(C_G)$ and $R_I(C_G, t)$ are the rates of glucose consumption and insulin production by the islets, respectively. Due to the nonlinear form of the glucose and insulin kinetics, an analytical solution is not possible. The axial diffusion terms, although of much less importance than the radial diffusion terms, were included for the sake of completeness.

Insulin secretion kinetics

Insulin production kinetics by islets has been shown to display a biphasic response to a glucose challenge (Grodsky, 1972; Inoue et al., 1992; Lacy et al., 1991). A model has been developed (Pillarella, 1989) to represent the kinetic response, based on a two-compartment approach proposed by Grodsky (Grodsky, 1972). Although this model is consistent with the biphasic insulin-secretion data, it results in unrealistically high initial insulin-secretion rates during the first phase. Moreover, the parameters in Pillarella's model were calculated using rat, rather than porcine, data. While both porcine and rat islets show a biphasic response to glucose stimulation, the secretion rate per islet tends to be lower in tissue from pigs compared to rats (Inoue et al., 1992; Lim and Sun, 1980; Marchetti et al., 1994; Nomora et al., 1984). With a modification to include a linear increase in insulin secretion during the first phase, the kinetic expression for insulin secretion becomes

$$R_I(C_G,t)=m_0=\alpha+\beta t, \qquad \text{when} \quad t<t^*$$

and

$$R_I(C_G,t)=m_1+m_2, \qquad \text{when} \quad t>t^*, \quad (3)$$

where

$$m_1=A\exp(-\alpha_1(t-t_1^*))$$

$$m_2=B[1-\exp(-\alpha_2(t-t_2^*))]$$

and

$$A=\frac{V_{m,1}(C_G-C_{G,1})}{K_{m,1}+(C_G-C_{G,1})}, \qquad B=\frac{V_{m,2}(C_G-C_{G,2})}{K_{m,2}+(C_G-C_{G,2})}.$$

The kinetic parameters $V_{m,1}$, $V_{m,2}$, α, and β, time constants α_1 and α_2, and time delays t_1^* and t_2^*, were evaluated by fitting this model to experimental data obtained using porcine islets (Inoue et al., 1992). Inoue's results were obtained from a single step increase in glucose concentration. The evaluation of the parameters reflecting glucose dependency ($K_{m,1}$, $K_{m,2}$, $C_{G,1}$, and $C_{G,2}$) require measurements of insulin secretion rates in response to a variety of glucose step increases. Since these types of data have not yet been reported for porcine islets, the insulin-secretion data from rat islets (Nomura et al., 1984) were used. Details are provided elsewhere (Belovich et al., 1996). Parameter values are given in Table 1.

Insulin kinetics in rats have been shown to be dependent on oxygen concentration (Dionne et al., 1991) as well as glucose. Although the oxygen concentration in the fiber can be considered to be at steady state, the value of the insulin secretion may be lower at the center of the fiber because of possible oxygen limitation. The effect of oxygen on insulin production is not considered here.

Glucose consumption kinetics

The consumption of glucose by the islets may be expected to cause a reduction in glucose concentration in the fiber, which may then lead to a lower insulin stimulation. Few measurements of glucose consumption by islets are available. In 1981, Trus and colleagues (Trus et al., 1981) suggested that the glucose consumption rate (R_G) by rat islets could be represented by the following model:

$$R_G(C_G)=0.85\,R_{G,\text{high}}+0.15\,R_{G,\text{low}} \quad (4)$$

where

$$R_{G,\text{high}}=\frac{V_{m,\text{high}}\,C_G}{K_{m,\text{high}}+C_G}$$

$$R_{G,\text{low}}=\frac{V_{m,\text{low}}\,C_G}{K_{m,\text{low}}+C_G}.$$

Since similar data are not available for porcine islets, this model was used in this work to represent the glucose con-

Table 1. Parameter Values Used in the "Typical Case" Model Calculations

	Value	Description	Reference
$C^b_{G,\text{fast}}$	87 mg/dL	Fasting glucose concentration in the blood	Segre et al., 1972
$C^b_{G\_\text{init}}$	230 mg/dL	Glucose concentration in the blood after a meal	Segre et al., 1972
$C^b_{I,\text{fast}}$	45 mU/mL	Fasting insulin concentration in the blood	Segre et al., 1972
D_{I-a}	2.82×10^{-4} mm^2/s	Diffusion coefficient of insulin through alginate	Moller, 1988
D_{G-a}	6.1×10^{-4} mm^2/s	Diffusion coefficient of glucose through alginate	Moller, 1988
$D_{I,\text{tissue}}$	1.5×10^{-4} mm^2/s	Diffusion coefficient of insulin through tissue	Mosekilde et al., 1989
D_{G-b}	9.1×10^{-4} mm^2/s	Diffusion coefficient of glucose through blood	*Handbook of Physiology*, 1977
D_{I-b}	1.46×10^{-4} mm^2/s	Diffusion coefficient of insulin through blood	Binder, 1983
$C_{G,1}$	60 mg/dL	Insulin secretion kinetics	Belovich, 1996
$K_{m,1}$	40 mg/dL	Insulin secretion kinetics	Belovich, 1996
$V_{m,1}$	0.17 μU/islet/min	Insulin secretion kinetics	Belovich, 1996
t_1^*	174 s	Insulin secretion kinetics	Belovich, 1996
α_1	0.0216 l/s	Insulin secretion kinetics	Belovich, 1996
$C_{G,2}$	60 mg/dL	Insulin secretion kinetic	Belovich, 1996
$K_{m,2}$	71.3 mg/dL	Insulin secretion kinetics	Belovich, 1996
$V_{m,2}$	0.23 μU/islet/min	Insulin secretion kinetics	Belovich, 1996
t_2^*	311 s	Insulin secretion kinetics	Belovich, 1996
α_2	0.00106 l/s	Insulin secretion kinetics	Belovich, 1996
β	0.0507 μU/islet/min^2	Insulin secretion kinetics	Belovich et al., 1996
a	1.15×10^{-8} l/s^2	Eq. 12	
b	31,748 s	Eq. 12	
$V_{m,\text{high}}$	2.72×10^{-8} mg/islet/s	Glucose consumption kinetics	Trus et al., 1981
$K_{m,\text{high}}$	200 mg/dL	Glucose consumption kinetics	Trus et al., 1981
$V_{m,\text{low}}$	1.34×10^{-8} mg/islet/s	Glucose consumption kinetics	Trus et al., 1981
$K_{m,\text{low}}$	3.87 mg/dL	Glucose consumption kinetics	Trus et al., 1981
$P_{m,G}$	4.5×10^{-4} mm/s	Glucose permeability in membrane	Ward et al., 1993
$P_{m,I}$	1.1×10^{-4} mm/s	Insulin permeability in membrane	Ward et al., 1993
v_b	0.75 mm/s	Average blood velocity in a capillary	Cooney, 1976
r_{cap}	0.0075 mm	Radius of a capillary	Cooney, 1976
ρ_{blood}	1.056	Specific gravity (25/4C) of the blood	Cooney, 1976
μ_{blood}	3.0 cp	Viscosity of the blood	Cooney, 1976
C_D	300 1/mm^2	Capillary density in the tissue	Cooney, 1976
r_∞	1.65 mm	Radius of the tissue area affected by a single fiber	Appendix
δ	.578 mm	Distance between fiber and position of median insulin cone	Appendix
r_{fiber}	0.50 mm	Radius of the fiber	
L	20 mm	Length of the film	
y_{islet}	40,000 islet/mL	Islet concentration in the fiber	

sumption kinetics. The kinetic parameters ($V_{m,\text{high}}$, $V_{m,\text{low}}$, $K_{m,\text{high}}$, and $K_{m,\text{low}}$) were calculated from the data from (Trus et al., 1981), and are given in Table 1.

Transport phenomena in the capillary

The model for the transport phenomena in the capillary is based on the diffusion of solutes from the hollow fiber to the blood, and convective and diffusive transport in the capillary blood. The conservation equations for glucose and insulin are

$$\left[-A_{\text{flow}}v_b\frac{\partial C^c_G}{\partial z}+A_{\text{flow}}D_{G-b}\frac{\partial^2 C^c_G}{\partial z^2}+2\pi r_{\text{fiber}}k_{mG}(C_G|_{r=r_{\text{fiber}}}-C^c_G)\right]=A_{\text{flow}}\frac{\partial C^c_G}{\partial t} \quad (5)$$

$$\left[-A_{\text{flow}}v_b\frac{\partial C^c_I}{\partial z}+A_{\text{flow}}D_{I-b}\frac{\partial^2 C^c_I}{\partial z^2}+2\pi r_{\text{fiber}}k_{mI}(C_I|_{r=r_{\text{fiber}}}-C^c_I)\right]=A_{\text{flow}}\frac{\partial C^c_I}{\partial t} \quad (6)$$

$$A_{\text{flow}}=A_{\text{tissue}}C_D\pi r^2_{\text{cap}}, \quad (7)$$

where C^c_G is the glucose concentration in the capillary blood, C^c_I is the insulin concentration in the capillary blood, D_{G-b} and D_{I-b} are the diffusion coefficients of glucose and insulin in blood, respectively, A_{flow} is the sum of the capillary cross-sectional areas, and A_{tissue} is the tissue area that is assumed to be influenced by the presence of the fiber (see the Appendix). The capillary density (C_D) is used to represent different regions of the body. A typical capillary radius (r_{cap}) is used, and the internal radius of the fiber (r_{fiber}) is a design parameter. The mass-transfer coefficient (K_{mI}) accounts for resistances between the alginate within the fiber and the blood in the capillaries.

Initial/boundary conditions

Fiber Equations. The initial insulin concentration in the fiber (the initial condition for Eq. 2) is assumed to be equal to the insulin concentration in the bloodstream at fasting conditions ($C^b_{\text{I,fast}}$):

$$C_I(0,r,z)=C^b_{I,\text{fast}}.$$

The assumption of symmetry yields the boundary condition at the center of the fiber:

$$r = 0 \qquad \frac{\partial C_I}{\partial r} = 0.$$

No accumulation is assumed in the tissue region:

$$r = r_{\text{fiber}} \qquad -D_{I-a}\frac{\partial C_I}{\partial r} = k_{mI}[C_I(t) - C_I^c(t)].$$

The overall mass-transfer coefficient, k_{mI}, accounts for the resistance of the fiber membrane, the resistance of the tissue, and the film mass-transfer coefficient through a blood boundary layer:

$$\frac{1}{k_{mI}} = \frac{1}{P_{mI}} + \frac{1}{P_{tI}} + \frac{1}{k_{cI}}. \tag{8}$$

The fiber permeability, P_{mI}, has been measured for several membrane types (see the next section). The film mass-transfer coefficient, k_{cI}, is based on flow through cylindrical tubes (Yang and Cussler, 1986):

$$\frac{2k_{cI}r_{\text{cap}}}{D_{I-b}} = 1.64\left(\frac{4v_b r_{\text{cap}}^2}{L_{\text{cap}}D_{I-b}}\right)^{1/3}, \tag{9}$$

where L_{cap} is the length of a typical capillary. The derivation of the tissue permeability (P_{tI}) is given in the Appendix.

Since both ends of the fiber are sealed, the axial boundary conditions can be formulated as:

$$z = 0 \qquad \frac{\partial C_I}{\partial z} = 0$$

$$z = L \qquad \frac{\partial C_I}{\partial z} = 0$$

where L is the fiber length.

Blood Side Equations. The initial condition for the insulin transport equation in the capillary blood (Eq. 6) is the insulin concentration at fasting conditions:

$$C_I^c(0, r) = C_{I,\text{fast}}^b.$$

The boundary conditions for Eq. 6 in the axial direction are given by the Danckwerts condition (Bischoff, 1961):

$$z = 0 \qquad -D_{I-b}\frac{\partial C_I^c}{\partial z} = v_b[C_I^b(t) - C_I^c(t)]$$

$$z = L \qquad \frac{\partial C_I^c}{\partial z} = 0,$$

where $C_I^b(t)$ is the insulin concentration in the bloodstream upstream of the fiber's leading edge

The boundary and initial conditions for the glucose equations (Eqs. 1 and 5) have the same form as those given previously for insulin.

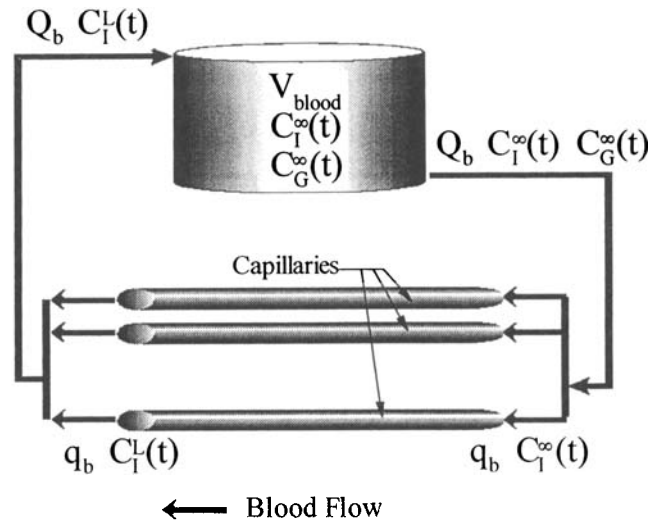

Figure 2. Circulatory system.

Circulatory system model

The transport model is based on a single fiber, assuming that each fiber behaves independently. To calculate the total amount of insulin secreted, the flux from each individual fiber is multiplied by the total number of fibers. The average insulin concentration in the bloodstream is derived based on an idealization of the circulatory system as shown in Figure 2. The bloodstream is represented by a single, well-mixed compartment, hereafter called the "blood compartment." The dynamic mass balance on insulin in the blood compartment is given by

$$\frac{dC_I^b(t)}{dt} = \frac{Q_b}{V_{\text{blood}}}[C_I^L(t) - C_I^b(t)], \tag{10}$$

where V_{blood} is the volume of the blood compartment, $C_I^L(t)$ is the insulin concentration at the end of the capillary, and Q_b is the total blood flow rate around the device, given by

$$Q_b = N_{\text{fiber}} \cdot q_b = N_{\text{fiber}} \cdot A_{\text{flow}} \cdot v_b, \tag{11}$$

where N_{fiber} is the number of fibers used in the artificial pancreas design, and q_b is the blood flow rate around each fiber. The initial condition for Eq. 10 is the fasting insulin concentration:

$$C_I^b(0) = C_{I,\text{fast}}^b.$$

Parameter values

The values of all parameters used in the model are shown in Table 1. The selection of the diameter and length of the fiber was based on typical values reported in the literature (Altman, 1988; Penfornis et al., 1990; Lacy et al., 1991; Lanza et al., 1991; Ward et al., 1993). The fiber permeability for glucose ranges from 1.2×10^{-2} mm/s for AN69 membrane [calculated from data in (Kessler et al., 1992)] to 4.5×10^{-4} mm/s for a nonporous elastomeric polymer membrane (Ward et al., 1993). The fiber permeability for insulin ranges from

5.5×10^{-4} mm/s for an untreated AN69 membrane (Kessler et al., 1992) to 1.1×10^{-4} mm/s for the nonporous elastomeric membrane (Ward et al., 1993), to 6.5×10^{-5} mm/s for an implanted AN69 membrane after 7 days (Kessler et al., 1992). Average values of these permeabilities are used in the simulations.

The initial glucose concentration in the fiber was assumed to be equal to the blood glucose concentration in the fasting state, $C^b_{G,\text{fast}}$, which is typically $80 \sim 100$ mg/dL (Granner, 1988). Initial insulin concentrations in the fiber and blood are assumed to be equal to the typical value in the bloodstream in the fasting state (Segre et al., 1972). After a meal, the glucose concentration in the bloodstream rapidly increases to approximately 230 mg/dL, and then gradually decreases with time as the glucose is taken up by the liver, adipose, and other tissue. This glucose uptake is stimulated by the presence of insulin. Since mathematical modeling of the feedback effect of insulin on glucose would greatly increase the complexity of the model, a simplified approach was chosen, where an empirical expression represents the glucose concentrations in the bloodstream following a meal. This glucose concentration upstream from the fiber $[C^b_G(t)]$, is given by

$$C^b_G(t) = C^b_{G,\text{fast}} + [C^b_{G,\text{init}} - C^b_{G,\text{fast}}]\exp[-at(t+b)] \quad (12)$$

with the parameters (a, b, and $C^b_{G,\text{init}}$) obtained by fitting this model to experimental measurements of glucose concentrations in nondiabetic patients following a meal (Segre et al., 1972). Equation 12 serves as the input to the bioartificial pancreas model, stimulating insulin secretion.

Measurements of insulin concentrations in the bloodstream in nondiabetic human patients during a glucose-tolerance test have shown that insulin concentration increases from 45 to 76 mU/mL within the first 25 min (Segre et al., 1972). These measurements are used as a criterion for determining the number of fibers needed in the bioartificial pancreas. The value of N_{fiber} was adjusted until the insulin concentration in the blood predicted by the simulation approximated these experimental values. For the typical case parameter values, N_{fiber} was found to equal 1,500.

Xenotransplantation studies using rat islets have used islet concentrations in the fiber of around 25,000 islets/mL (Lacy et al., 1991) to 138,000 islets/mL (Zekorn et al., 1990). Given an average porcine islet diameter of 150 μm, the maximum islet loading is 300,000 islets/mL. Concentrations between 40,000 and 80,000 islets/mL were selected for use in the simulations.

The equations were solved numerically using linear finite-element and finite-difference techniques (Buladi, 1994).

Results

All calculations are performed using the parameters in Table 1, defined as the "typical case," except where otherwise noted. Figure 3a shows glucose radial concentration profiles inside the fiber at different times. Initially, the glucose concentration decreases from the fiber wall to the center of the fiber, due to the diffusion of the glucose into the fiber. A completely flat profile will never be reached because of the consumption of glucose by the islets.

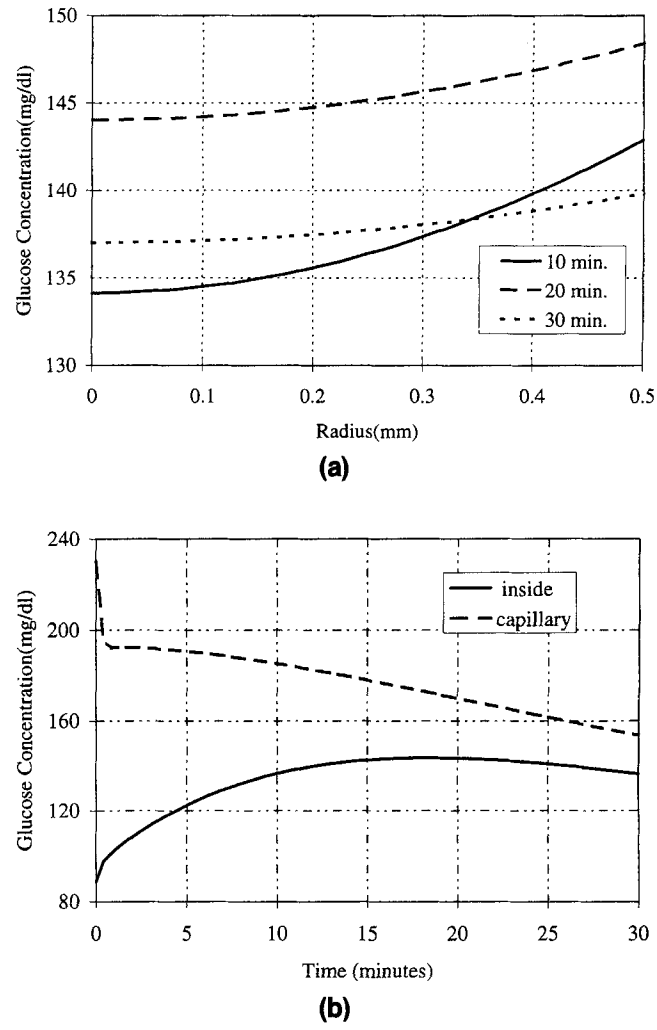

Figure 3. Glucose concentrations, using the typical case parameters from Table 1.

(a) Radial glucose concentration profiles in the fiber (C_G). (b) Glucose concentrations at the end of the fiber and just inside the fiber membrane [$C_G(r = r_{\text{fiber}}, z = L)$], and in the capillary [$C^c_G(z = L)$].

Figure 3b shows the glucose concentration at the end of the fiber length, just inside the fiber wall, and the concentration in the capillaries at the same length. The concentration in the capillaries decreases in a manner similar to the time profile in the blood compartment (C^b_G), which is used as the boundary condition, demonstrating that the glucose concentration in the capillaries is controlled by the blood compartment. In the fiber, the glucose concentration is limited by diffusive transport in the first 17 minutes. After this point, the glucose concentration decreases in the same manner as in the capillaries. A steady-state glucose profile is never reached because of the changing glucose concentration in the bloodstream.

Insulin radial concentration profiles during the first seven minutes following a glucose challenge are displayed in Figure 4a, and the insulin concentration in the capillaries in Figure 4b. From these figures one can observe a large concentration gradient between the inside of the fiber and the tissue region. Recall that the intrinsic insulin secretion kinetics dis-

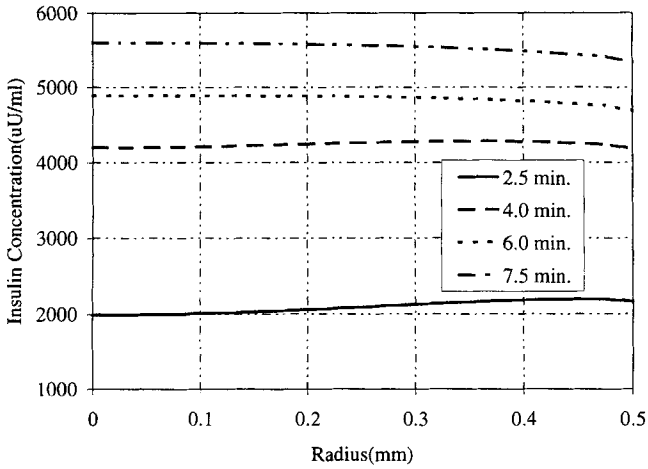

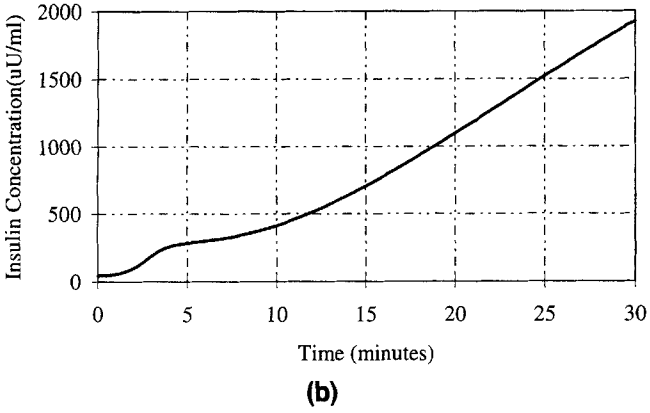

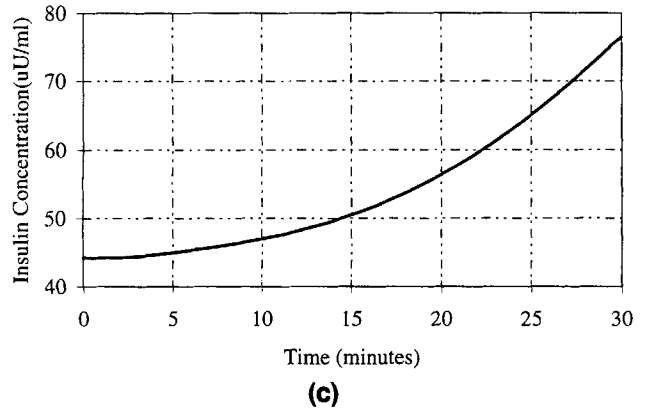

Figure 4. Insulin concentrations, using the typical case parameters from Table 1.

(a) Radial insulin concentration profiles in the fiber (C_I). (b) Capillary insulin concentration at $z = L$ [$C_I^c(z = L)$]. (c) Blood compartment insulin concentration (C_I^b).

plays a peak in insulin secretion at about 3 minutes following a glucose challenge, and then increases gradually again over the next 15 minutes (Inoue et al., 1992). This kinetic behavior is manifested in the insulin concentration in the capillaries surrounding the fiber (Figure 4b), where a steep increase in concentration is observed between the second to fourth minute, and then a slower rate of increase occurs in the next 26 minutes. Overall, the kinetic behavior is hidden by the transport phenomena, since the insulin in the blood compartment increases monotonically, and does not show a local maximum (Figure 4c).

Capillary density

Variation in the capillary density is used to represent the effect of implantation site on the insulin dynamics. It is assumed that subcutaneous tissue has less blood flow, and thus a lower capillary density, than the intraperitoneal site. Two densities were considered: 300 (the typical case value) and 1,500 capillaries/mm^2 tissue, and the results are shown in Figure 5. Increasing the capillary density causes an approximate 4-fold decrease in the concentration in the capillary (Figure 5a), since the insulin is distributed into more capillaries. This lower concentration in the capillary causes a greater driving force for insulin transport, so that the concentration in the blood compartment increases. However, this increase is only noticeable after around 12 minutes, and only by about 4%, for a five-fold increase in blood flow (Figure 5b). Consequently, it appears that implantation site, in terms of blood

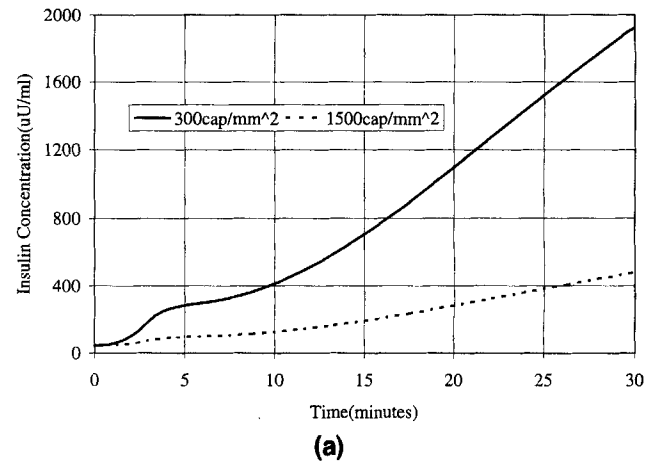

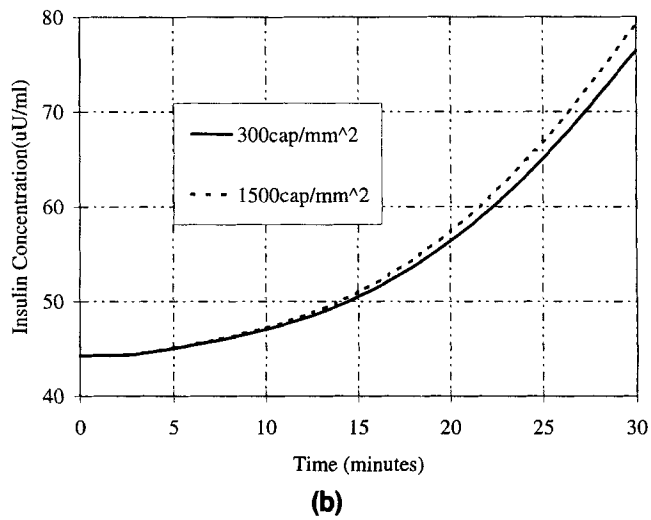

Figure 5. Effect of capillary density on (a) capillary insulin concentration at $z = L$ [$C_I^c(z = L)$], and (b) blood compartment insulin concentration (C_I^b).

flow rate, will have little effect on the response of the bioartificial pancreas. However, the model does not address other differences in implantation site, such as differences in oxygen tension, or the propensity for collagen or fibroblast accumulation on the membrane surface. Indeed, it has been shown that with a specific membrane processing technique, subcutaneous implants can be as effective as intraperitoneal implants in the treatment of diabetic mice, while with a different processing technique, transplant performance in the subcutaneous location is significantly poorer than in the intraperitoneal location (Lacy et al., 1991).

Membrane permeability

As described before, membrane permeabilities for both glucose and insulin can range over an order of magnitude, depending on the type of membrane. Figure 6 shows the effect of the insulin permeability ranging from 5.0×10^{-5} to 5.0×10^{-4} mm/s, while glucose permeability is kept at the typical case value. As expected, a larger permeability results in a dramatic increase (60%) in insulin concentration in the capillary (Figure 6a), as well as a 32% increase in concentration in the blood compartment (Figure 6b). The higher permeability causes the transport resistance of the fiber membrane to becomes less limiting, as shown by the increase in prominence of the two-phase kinetic response in the capillary. However, in the blood compartment, transport limitations still dominate even for the high permeability.

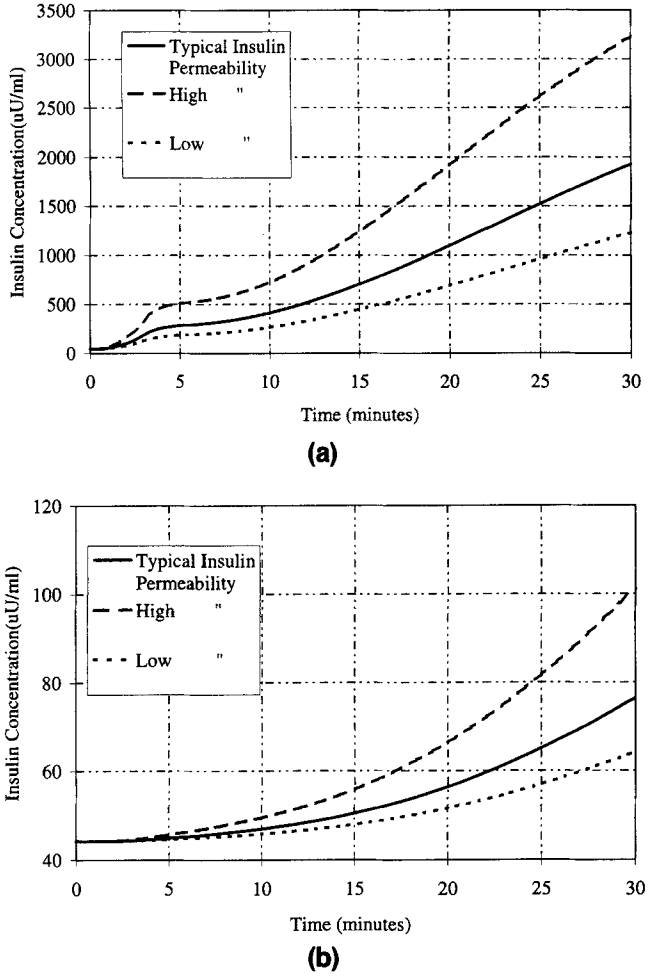

Figure 6. Effect of membrane insulin permeability on (a) capillary insulin concentration at $z = L$ [$C_I^c(z = L)$], and (b) blood compartment insulin concentration (C_I^b).

Low P_{mI} is 5.0×10^{-5} mm/s, high P_{mI} is 5.0×10^{-4} mm/s, and typical case is 1.06×10^{-4} mm/s.

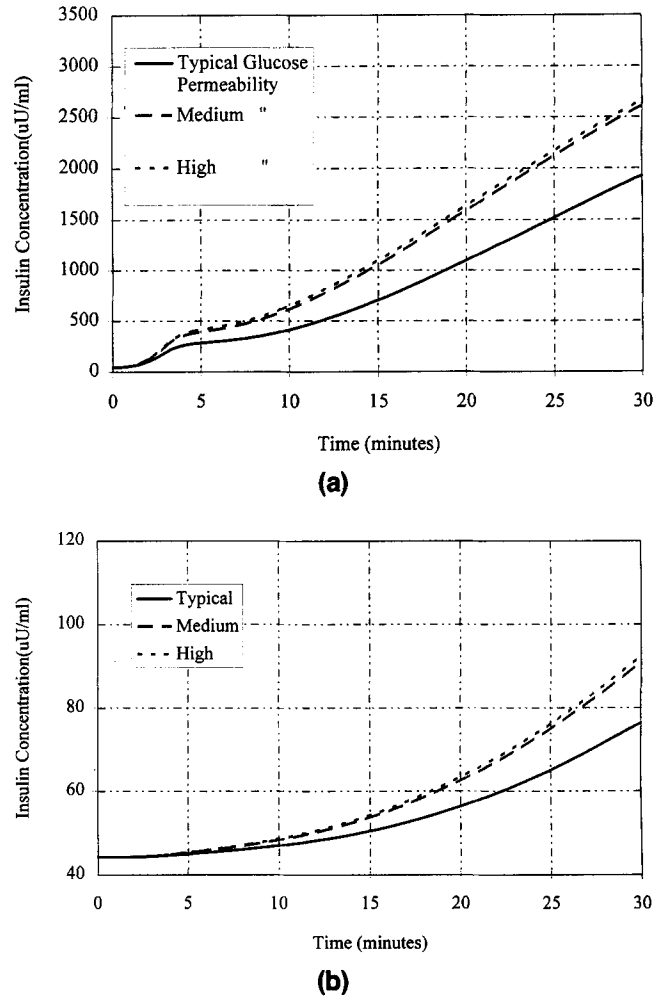

Figure 7. Effect of membrane glucose permeability on (a) capillary insulin concentration at $z = L$ [$C_I^c(z = L)$], and (b) blood compartment insulin concentration (C_I^b).

Typical case P_{mG} is 4.48×10^{-4} mm/s, medium P_{mG} is 5.0×10^{-3} mm/s, and high P_{mG} is 5.0×10^{-2} mm/s.

Results using membrane glucose permeabilities between 4.5×10^{-4} and 5.0×10^{-2} mm/s, while insulin permeability is kept at the typical case value, are shown in Figure 7. These results show that increasing the glucose permeability above 5.0×10^{-3} mm/s has little effect on the bioartificial pancreas performance.

Fiber diameter

In this section, the effects of changes in fiber diameter on insulin response are examined. Calculations are performed, keeping the volume of alginate constant in the bioartificial pancreas. Thus, for fiber diameter of 0.5 mm, N_{fiber} is 2,600,

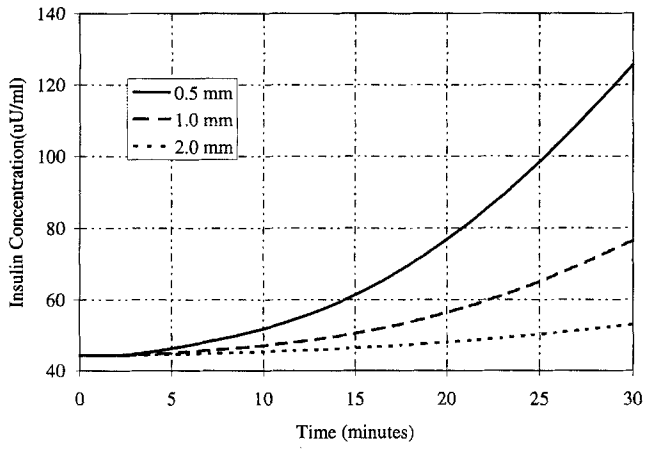

Figure 8. Effect of fiber diameter on insulin concentration in the blood compartment (C_I^b).

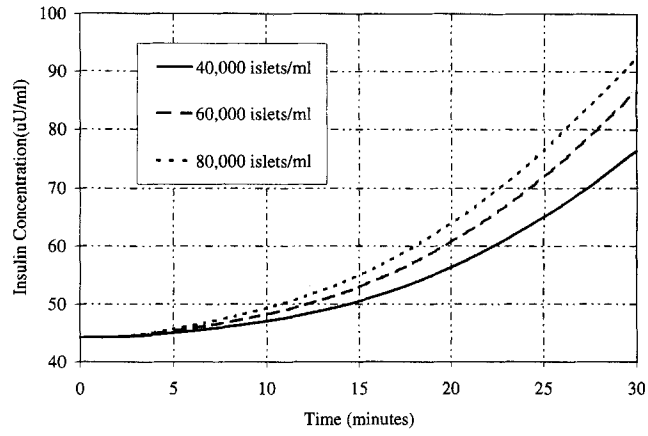

Figure 10. Effect of islet concentration, in islets/mL, on the insulin concentration in the blood compartment (C_I^b).

and for fiber diameter of 2.0 mm, N_{fiber} is 375. The dynamics of the insulin concentration in the blood compartment (Figure 8) for three different fiber diameters appears identical within the first 4–5 minutes. After 5 minutes, the insulin concentration dynamics begin to deviate significantly from each other. This characteristic of the dynamics is a result of the insulin-secretion kinetics—during the first phase insulin is secreted at high rate and, as a result of this large initial gradient, mass transport is very efficient. After the first phase, mass transport dominates the dynamics and the smaller fibers, with a larger area-to-volume ratio (and larger gradients due to their cylindrical nature), are more efficient in raising the insulin concentration in the blood compartment. Although the insulin reaction rate still plays an important role in determining the insulin response time, mass transport limitations appear to be the dominant factor in the long-time response.

Fiber length

The influence of the fiber length on the insulin response time is shown in Figure 9. In these calculations, the number of fibers was reduced to 750 to keep the volume of alginate constant. From the figure, it appears that shorter fibers have a slight advantage over the longer fibers. This results occurs because the shorter fibers demonstrate a larger concentration gradient, and therefore faster transport to the blood compartment.

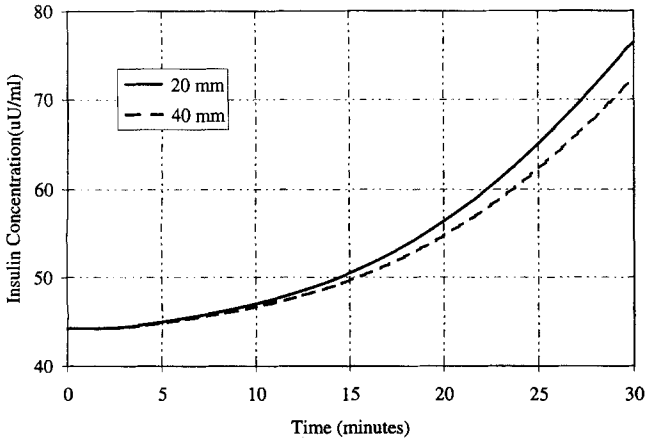

Figure 9. Effect of fiber length on insulin concentration in the blood compartment (C_I^b).

Islet concentration

The effect of islet concentration, for a constant number of fibers (1,500) is given in Figure 10. As expected, larger islet concentration results in higher insulin concentration in the bloodstream; however, the result is not directly proportional to the number of islets, because of the decrease in transport gradients at higher concentrations.

Mass-transport limitations

The advantage of constructing a detailed mathematical model is that it allows one to quantify the influence of the various transport processes on the desired outcome. These transport processes consist of radial and axial diffusion in the gel within the fiber, axial convection and diffusion in the capillary, and convection in the bloodstream. In addition, radial diffusion through the fiber membrane, the tissue, and the thin film in the capillary is characterized by an overall mass-transfer coefficient that contains terms for each of these resistances (Eq. 8). The effect of blood velocity and permeability on the different terms in Eq. 8 are shown in Tables 2 and 3. Analysis of these terms identifies the controlling transport process.

Table 2. Boundary-Layer Resistance Values and Overall Mass-Transfer Coefficients of Glucose for Different Membrane Permeabilities and Blood Velocities (in mm/s)*

V_b (mm/s)	k_{cG} (mm/s)	k_{mG} ($P_{mG} = 4.45\times10^{-4}$) (mm/s)	k_{mG} ($P_{mG} = 5\times10^{-3}$) (mm/s)	k_{mG} ($P_{mG} = 5\times10^{-2}$) (mm/s)
0.075	2.39×10^{-3}	3.77×10^{-4}	1.62×10^{-3}	2.28×10^{-3}
0.75	5.16×10^{-3}	4.12×10^{-4}	2.54×10^{-3}	4.67×10^{-3}
7.5	1.10×10^{-2}	4.31×10^{-4}	3.45×10^{-3}	9.09×10^{-3}

*The fiber diameter and insulin permeability are kept constant at the typical case values.

Table 3. Boundary-Layer Resistance Values and Overall Mass-Transfer Coefficients of Insulin for Different Membrane Permeabilities and Blood Velocities (in mm/s)*

V_b (mm/s)	k_{cI} (mm/s)	k_{mI} ($P_{mI} = 5.0\times10^{-5}$) (mm/s)	k_{mI} ($P_{mI} = 1.06\times10^{-4}$) (mm/s)	k_{mI} ($P_{mI} = 5.0\times10^{-4}$) (mm/s)
0.075	7.06×10^{-4}	3.96×10^{-5}	6.80×10^{-5}	1.38×10^{-4}
0.75	1.52×10^{-3}	4.08×10^{-5}	7.17×10^{-5}	1.54×10^{-4}
7.5	3.28×10^{-3}	4.14×10^{-5}	7.36×10^{-5}	1.62×10^{-4}

*The fiber diameter and glucose permeability are kept constant at the typical case values. The tissue permeability is kept constant at 2.6×10^{-4} mm/s.

As shown in Table 2 (for glucose), an increase in velocity gives rise to an increase in K_{cG}, and thus a decrease in the boundary layer resistance, as expected from Eq. 9. However, the change in the overall mass-transfer coefficient is negligible for low permeabilities. If the capillary velocity is increased by a factor of 10 for medium permeabilities, the overall mass-transfer resistance declines 35%. The change in the overall resistance is 51% for the high-permeability membrane when the same change in the capillary blood velocity is considered. In conclusion, at low to medium membrane permeabilities, the membrane is the limiting resistance for glucose transport. At high permeability, transport in the capillary, rather than the fiber membrane, is limiting. This result is echoed by Figure 7a where there is little change in the insulin dynamics between medium and high glucose permeabilities.

Table 3 shows that blood velocity has little effect on the insulin mass-transfer coefficient. At low to medium insulin membrane permeabilities, the membrane resistance is controlling. At high membrane permeability, the tissue resistance becomes controlling.

Based on the results in Tables 2 and 3 one would expect that for the typical case parameter values (i.e., low glucose permeability, and medium insulin permeability), that blood velocity would have a small effect on insulin dynamics. However, Figure 11 shows that the effect of blood velocity on insulin dynamics in the capillary (Figure 11a) and blood compartment (Figure 11b) can be quite significant. This seemingly contradictory result occurs because blood velocity contributes to convective transport in the capillary, as well as diffusive transport.

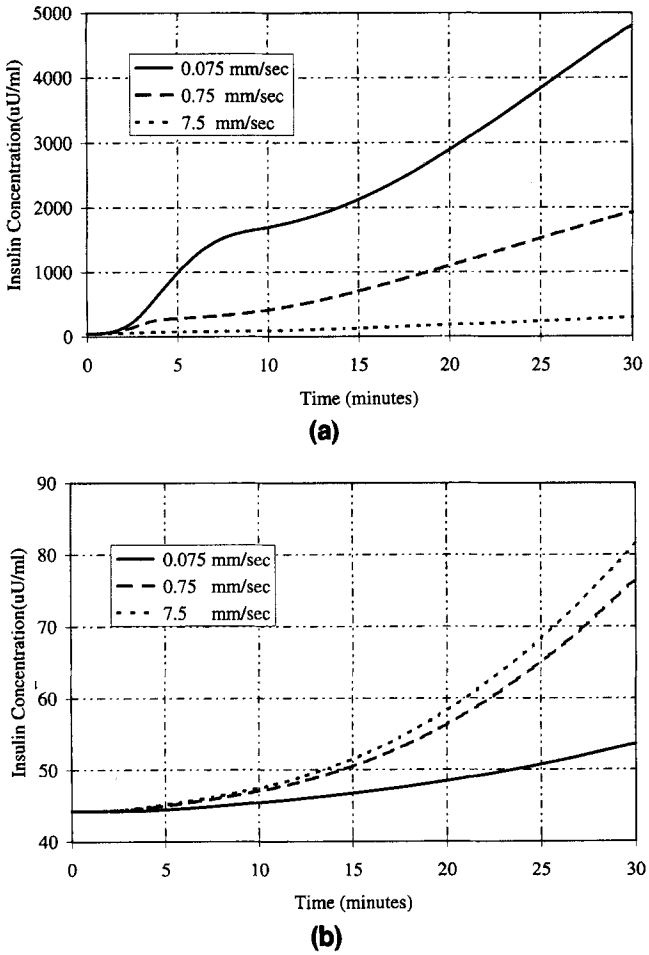

Figure 11. Effect of blood velocity on the (a) capillary insulin concentration at $z = L$ (C_I^c), and (b) blood compartment insulin concentration (C_I^b).

Glucose consumption

Figure 12 illustrates the effect of glucose consumption by the islets on the insulin concentration dynamics in the blood compartment. The consumption terms causes the local glucose concentration around the islets to be reduced, and thus reduces the insulin secretion rate. The reduction in insulin concentration in the bloodstream, although small, is not neglible, and indicates that glucose consumption should be accounted for when designing the device.

Discussion

The extravascular bioartificial pancreas, constructed using design parameters given in Table 1, would have a volume of alginate of 23.6 mL, and contain 942,000 porcine islets. The total volume of the device, assuming a fiber wall thickness of 0.1 mm, would be 33.9 mL. A device of this size may be too

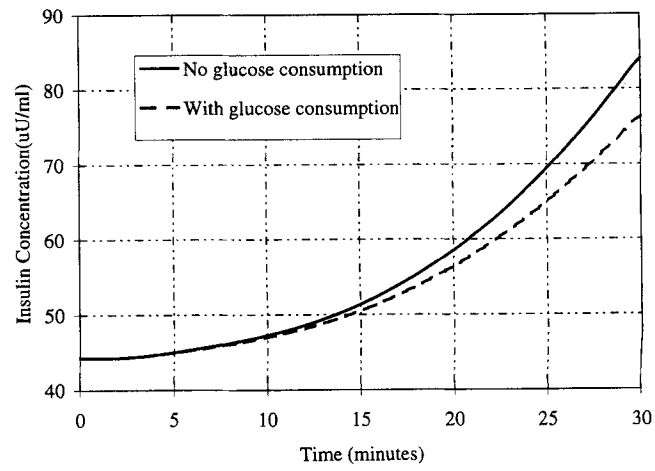

Figure 12. Insulin concentration in the blood compartment (C_I^b), calculated both with and without glucose consumption by the islets.

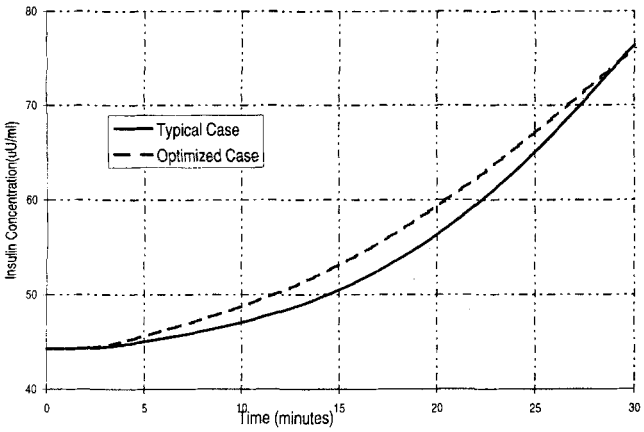

Figure 13. Insulin concentration in the blood compartment (C_I^b), for the typical case parameters given in Table 1, and for the optimized design.

large to be implanted. However, the simulations presented here have identified specific ways by which the design can be improved.

The performance of the bioartificial pancreas was found to be most sensitive to the permeability of the hollow-fiber membrane. Thus, it would be desirable to select a membrane that is very porous and thin, within the constraints of providing immunoisolation and physical strength. However, as shown in Figure 7, when the permeability becomes greater than 10^{-3} mm/s, transport processes other than the membrane become limiting. The performance is also sensitive to the fiber diameter. Narrow fibers have a larger surface-to-volume ratio, and thus better transport characteristics. For this reason, spherical beads will provide better transport properties, but are subject to the limitations described in the Introduction. A modification of the model presented here to represent spherical geometry would allow one to quantify the relative advantage of the spherical beads over hollow fibers. The number of capillaries around the implant was shown to have little effect on performance, but the velocity of the blood in the region of the implant has a significant effect. The insulin kinetics plays a major role in the system performance. The results presented here are based on porcine-insulin kinetic data, which have become available relatively recently. Although insulin production by porcine islets displays a biphasic response, the transport considerations dampen the response so that a monotonic increase in insulin concentration is observed in the overall blood compartment.

Based on the simulation results shown in the previous section, the design of the bioartificial pancreas can be optimized, within known physical constraints. The design can be greatly improved by increasing the membrane permeabilities to 5.0×10^{-3} mm/s for glucose and 5.0×10^{-4} mm/s for insulin, by decreasing the fiber inner diameter to 0.5 mm, and by increasing the islet concentration to 80,000 islets/mL. The insulin dynamics using these parameters are shown in Figure 13. With these design parameters, only 600 fibers are needed to reach a target insulin concentration in the bloodstream of 76 uU/mL. The volume of alginate would be 2.4 mL, containing 188,500 islets, and the total volume of the device would be 4.6 mL. For a point of comparison, the volume of a typical heart pacemaker, which is implanted under the skin, is about 30 mL. Therefore, a bioartificial pancreas of 4.6 mL is small enough to be practical for implanting into humans. The number of fibers can be increased to reduce the response time, if needed; the size of the unit would still be sufficiently small for human use.

As with all mathematical models, many simplifications were made. Since insulin clearance by the liver, as well as other "sinks" for insulin, were neglected, the predicted insulin concentration in the bloodstream is overestimated, perhaps up to a factor of 2. As time progresses following a meal, the insulin secretion rate first increases and then decreases, and the degradation of insulin increases, so that the insulin concentration in the bloodstream reaches a maximum. Since the model does not take into account these phenomena, the simulations do not predict a maximum. Clearly, then, the validity of the model will break down at longer time periods, and thus simulations up to only 30 minutes are shown.

The description of the capillary bed was also simplified in the model. However, the length of the capillaries has little effect on the overall results. A larger number of shorter capillaries would actually increase the rate of transport of the insulin to the bloodstream, since there would be a larger concentration gradient between the fiber and the capillary insulin concentration. Simulation results indicated that fiber wall permeability was the limiting factor in terms of insulin response. Therefore, an increase in the transport rate to the capillaries would only have a negligible effect on the overall BAP performance.

The insulin secretion kinetics were obtained from *in-vitro* data, where the islets were perfused with media oxygenated by a gas containing 95% oxygen. Implanted islets will experience an environment that is much lower in oxygen concentration. The lower oxygen concentration will most likely result in lower insulin secretion rates, as has been observed with rat islets (Dionne et al., 1991). Modifications of the model to account for the effect of oxygen limitations are currently underway. The modified model will be used to estimate the maximum fiber diameter that can be used without oxygen limitation, and to quantify the effect of fiber spacing on the performance.

This model does not address the subject of failure of the implanted device after a period of time. Several researchers have suggested that the device failure results from a reduction in the oxygen supply to the islets as the membranes become coated with proteins and cells. The modification of the model with oxygen transport as described earlier may provide some answers. Experimental research with vascularized membranes, and membranes that have minimal fibrotic growth, is ongoing and has shown positive results (Fournier, 1995; Ward, 1993). More research is also needed to determine if specific hormones are needed for insulin secretion that are not available to the implanted islets.

The results presented here are significant since they demonstrate that an extravascular device can be just as effective as convection-based, intravascular designs, without associated complications such as blood vessel grafts and blood flow across synthetic materials. These results confirm the recent trend in experimental work with animals, where research in extravascular devices has become more prevalent

than intravascular. To date, there have been no reports of islet xenotransplants to humans, so it is uncertain how the animal studies will be scaled-up to humans. The simulation results presented here suggest that an extravascular device can be feasible for human use based on criteria of response time and implant volume. The calculations should assist researchers who are designing and planning to test a bioartificial pancreas device in humans, by providing estimates of the number and size of fibers, the islet concentration, and membrane properties needed to obtain a physiological insulin response to a glucose challenge.

Acknowledgments

This work was supported by a Research Challenge Award from Cleveland State University. The authors also acknowledge valuable comments and suggestions by the reviewers of a preliminary version of this manuscript.

Literature Cited

Altman, J. J., "The Bioartificial Pancreas: Macroencapsulation of Insulin Secreting Cells in Hollow Fibers," *J. Diabetic Complications*, **2**(2), 68 (1988).

Beek, J., and E. Singer, "A Procedure for Scaling-Up a Catalytic Reactor," *Chem. Eng. Prog.*, **47,** 534 (1951).

Belovich, J. M., "Analysis of Insulin Secretion Kinetics," in preparation (1996).

Binder, C., "A Theoretical Model for the Absorption of Soluble Insulin," *Artificial Systems for Insulin Delivery*, P. Brunetti, ed., Raven Press, New York, p. 53 (1983).

Bischoff, K. B., "A Note on Boundary Conditions for Flow Reactors," *Chem. Eng. Sci.*, **16,** 131 (1961).

Buladi, B. M., *Transport Phenomena in a Bioartificial Pancreas*, M.S. Thesis, Cleveland State Univ., Cleveland, OH (1994).

Calafiore, R., G. Baste, A. Falorni, L. Avellini, and P. Brunetti, "Immunoisolation of Porcine Islets of Langerhans within Algin/Polyaminoacidic Microcapsules," *Horm. Matab. Res. Suppl.*, **25,** 213 (1990).

Clayton, H. A., R. F. L. James, and N. J. M. London, "Islet Microencapsulation: A Review," *Acta Diabetol.*, **30,** 181 (1993).

Cooney, D. O., *Biomedical Engineering Principles: An Introduction to Fluid, Heat and Mass Transport Processes*, Marcel Dekker, New York (1976).

Crider, J. E., and A. S. Foss, "Effective Wall Heat Transfer Coefficients and Thermal Resistances in Mathematical Models of Packed Beds," *AIChE J.*, **11,** 1012 (1965).

Darquy, A., D. Chicheportiche, F. Capron, C. Boitard, and G. Reach, "Comparative Study of Microencapsulated Rat Islets Implanted in Different Diabetic Models in Mice," *Horm. Metab. Res. Suppl.*, **25,** 209 (1990).

Dionne, K. E., C. K. Colton, and M. L. Yarmush, "A Microperifusion System with Environmental Control for Studying Insulin Secretion by Pancreatic Tissue," *Biotechnol. Prog.*, **7,** 359 (1991).

Fan, Y., X. P. Lum, X. W. Fu, L. Levesque, I. T. Tai, and A. M. Sun, "Reversal of Diabetes in BB Rats by Transplantation of Encapsulated Pancreatic Islets," *Diabetes*, **39,** 519 (1990).

Finlayson, B. A., *Nonlinear Analysis in Chemical Engineering*, McGraw-Hill, New York (1980).

Fritschy, W. M., G. H. J. Wolters, and R. van Schilfgaarde, "Effect of Alginate-Polylysine-Alginate Microencapsulation on In Vitro Insulin Release from Rat Pancreatic Islets," *Diabetes*, **40,** 37 (1991).

Fournier, R. L., *Basic Concepts of Biomedical Engineering*, Greyden Press, Columbus, OH (1995).

Granner, D. K., "Hormones of the Pancreas," *Harper's Biochemistry*, R. K. Murray et al., eds., Appleton & Lange, Norwalk, CT (1988).

Grodsky, G. M., "A Threshold Distribution Hypothesis for Packet Storage of Insulin and its Mathematical Modeling," *J. Clin. Invest.*, **51,** 2047 (1972).

Handbook of Physiology, American Physiological Society, Baltimore, MD (1977).

Hlavacek, V., and J. Votruba, *Chemical Reactor Theory: A Review*, Chap. 6, L. Lapidus and N. R. Amundson, eds., Prentice Hall, Englewood Cliffs, NJ (1977).

Inoue, K., Y. Gu, S. Shinohara, M. Kogire, M. Mitsuo, I. Nakai, H. Hayashi, K. Uchida, S. Maetani, Y. Ikada, and T. Tobe, "Isolation of Adult Pig Islet," *Int. J. Pancreatol.*, **12,** 73 (1992).

Jaffrin, M. Y., G. Reach, and D. Notelet, "Analysis of Ultrafiltration and Mass Transfer in a Bioartificial Pancreas," *J. Biomech. Eng.*, **110,** 1 (1988).

Kelsey, L. J., M. R. Pillarella, and A. L. Zydney, "Theoretical Analysis of Convective Flow Profiles in a Hollow-Fiber Membrane Bioreactor," *Chem. Eng. Sci.*, **45**(11), 3211 (1990).

Kessler, L., M. Aprahamian, M. Keipes, C. Damge, M. Pinget, and D. Poinsot, "Diffusion Properties of An Artificial Membrane Used for Langerhans Islets Encapsulation: An In Vitro Test," *Biomaterials*, **13**(1), 6 (1992).

Krestow, M., Z. P. Lum, I. T. Tai, and A. Sun, "Xenotransplantation of Microencapsulated Fetal Rat Islets," *Transplantation*, **51,** 651 (1991).

Lacy, P. E., O. D. Hegre, A. Gerasimidi-Vazeou, F. T. Gentile, and K. E. Dionne, "Maintenance of Normoglycemia in Diabetic Mice by Subcutaneous Xenografts of Encapsulated Islets," *Science*, **254,** 1782 (1991).

Lanza, R. P., D. H. Butler, K. M. Borland, J. E. Staruk, D. L. Faustman, B. A. Solomon, T. E. Muller, R. G. Rupp, T. Maki, A. P. Monaco, and W. L. Chick, "Xenotransplantation of Canine, Bovine, and Porcine Islets in Diabetic Rats without Immunosuppression," *Proc. Nat. Acad. Sci. U.S.A.*, **88,** 11100 (1991).

Lim, F., and A. M. Sun, "Microencapsulated Islets as Bioartificial Endocrine Pancreas," *Science*, **210,** 908 (1980).

Marchetti, P., D. W. Scharp, K. Pfiffner, C. J. Swanson, E. H. Finke, B. J. Olack, A. Gerasimidi-Vazeou, M. McLear, and P. E. Lacy, "Cryogenic Storage of Isolated, Purified Porcine Pancreatic Islets," *Transplantation*, **57,** 340 (1994).

Mikos, A. G., M. G. Papadaki, S. Kouvroukoglou, S. L. Ishaug, and R. C. Thomson, "Mini-Review: Islet Transplantation to Create a Bioartificial Pancreas," *Biotechnol. Bioeng.*, **43,** 673 (1994).

Moller, U., "Determination of Diffusion Coefficients of Insulin and Insulin Analogs in Relationship to Physical and Absorption Properties," *Diabetes*, **37,** 163A (1988).

Mosekilde, E., K. S. Jensen, C. Binder, S. Pramming, and B. Thorsteinsson, "Modeling Absorption Kinetics of Subcutaneous Injected Soluble Insulin," *J. Pharmacokinet. Biopharm.*, **17**(1), 67 (1989).

Nomura, M., M. Shichiri, R. Kawamori, Y. Yamasaki, N. Iwama, and H. Abe, "A Mathematical Insulin-Secretion Model and its Validation in Isolated Rat Pancreatic Islets Perifusion," *Comput. Biomed. Res.*, **17,** 570 (1984).

Penfornis, F., P. Icard, C. Gotheil, J. Boillot, C. Cornec, F. Barrat, J. J. Altman, and J. V. Cochin, "Bioartificial Pancreas in Pigs: I. Islet Immunoisolation," *Horm. Metab. Res. Suppl.*, **25,** 200 (1900).

Pillarella, M. R., and A. L. Zydney, "Theoretical Analysis of the Effect of Convective Flow on Solute Transport and Insulin Release in a Hollow Fiber Bioartificial Pancreas," *Trans. ASME*, **112,** 220 (1990a).

Pillarella, M. R., and A. L. Zydney, "Effect of Beta Cell Distribution on the Performance of a Bioartificial Pancreas," *Trans. ASAIO*, **36,** m715 (1990b).

Pillarella, M. R., *Solute Transport in Hollow Fiber Membranes and its Application to Hemofiltration and the Bioartificial Pancreas*, PhD Diss., Massachusetts Institute of Technology, Cambridge (1989).

Ramirez, C. A., M. Lopez, and C. L. Stephens, "In Vitro Perfusion of Hybrid Artificial Pancreas Devices at Low Flow Rates," *ASAIO J.*, **38**(3), M443 (1992).

Reach, G., "Bioartificial Pancreas," *Diabetic Med.*, **10,** 105 (1993).

Reach, G., and M. Y. Jaffrin, "Kinetic Modelling as a Tool for the Design of a Vascular Bioartificial Pancreas: Feedback between Modelling and Experimental Validation," *Comput. Methods Programs Biomed.*, **32,** 277 (1990).

Sarver, J. G., and R. L. Fournier, "Numerical Investigation of a Novel Spiral Wound Membrane Sandwich Design for an Implantable Bioartificial Pancreas," *Comput. Biol. Med.*, **20**(2), 105 (1990).

Sarver, J. G., R. L. Fournier, P. J. Goldblatt, T. L. Phares, S. E. Mertz, A. R. Baker, R. J. Mellon, J. M. Horner, and S. H. Selman, "Tracer Technique to Measure In Vivo Chemical Transport Rates

within an Implantable Cell Transplantation Device," *Cell Transplant.*, **4**, 201 (1995).
Segre, G., G. L. Turco, and G. Vercellone, "Modeling Blood Glucose and Insulin Kinetics in Normal, Diabetic and Obese Subjects," *Diabetes*, **22**(2), 94 (1972).
Sullivan, S. J., T. Maki, K. M. Borland, M. D. Mahoney, B. A. Solomon, T. E. Muller, A. P. Monaco, and W. L. Chick, "Biohybrid Artificial Pancreas: Long-Term Implantation Studies in Diabetic, Pancreatectomized Dogs," *Science*, **25**, 718 (1991).
Sun, Y. L., X. Ma, D. Zhou, I. Vacek, and A. M. Sun, "Porcine Pancreatic Islets: Isolation, Microencapsulation, and Xenotransplantation," *Artif. Organs*, **17**, 727 (1993).
Trus, M. D., W. S. Zawalich, P. T. Burch, D. K. Berner, V. A. Weill, and F. M. Matschinsky, "Regulation of Glucose Metabolism in Pancreatic Islets," *Diabetes*, **30**, 911 (1981).
Ward, R. S., K. A. White, C. A. Wolcott, A. Y. Wang, R. W. Kuhn, J. E. Taylor, and J. K. John, "Development of a Hybrid Artificial Pancreas with a Dense Polyurethane Membrane," *ASAIO J.*, **39**, m261 (1993).
Warnock, G. L., D. Ellis, R. V. Rajotte, I. Dawidson, S. Baekkeskov, and J. Egebjerg, "Studies of the Isolation and Viability of Human Islets of Langerhans," *Transplantation*, **45**, 957 (1988).
Weber, C. J., S. Zabinsi, T. Koschitzky, R. Rajotte, L. Wicker, L. Peterson, V. D'Agati, and K. Reemtsma, "Microencapsulated Dog and Rat Islet Xenografts into Streptozotocin-Diabetic and NOD Mice," *Horm. Metab. Res. Suppl.*, **25**, 219 (1990).
Yang, M. C., and E. L. Cussler, "Designing Hollow Fiber Contactors," *AIChE J.*, **32**, 1910 (1986).
Zekorn, T., M. Renardy, H. Planck, P. Zschocke, R. G. Bretzel, U. Siebers, and K. Federlin, "Experiments on a New Hollow Fiber Membrane for Immunoisolated Transplantation of Islets of Langerhans," *Horm. Metab. Res. Suppl.*, **25**, 202 (1990).

Appendix: Estimation of Lumped Tissue Resistance

Insulin or glucose radial mass transport in the tissue (and capillaries) surrounding the fiber is governed by

$$\frac{\partial C}{\partial t} = D_{\text{tissue}}\nabla^2 C - S(C)$$

subject to

$$D_{\text{tissue}}\frac{\partial C}{\partial r} = k_m(C - C^{\text{fiber}}) \qquad @\ r = r_{\text{fiber}}$$
$$\frac{\partial C}{\partial r} = 0 \qquad @\ r = r_\infty, \qquad \text{(A1)}$$

where C represents the concentration (of glucose/insulin) in the tissue; $S(C)$ stands for a sink/source term that represents the transport of either glucose *from* the blood system, or insulin *to* the blood system; C^{fiber} is the concentration (of glucose/insulin) at the fiber membrane on the alginate side; and r_∞ is a radial position far enough from the fiber such that effectively no radial mass transport, of glucose/insulin, will be observed at r_∞. The calculation/estimation of r_∞ is explained later in this Appendix.

The preceding equation will be better suited for mathematical analysis if rewritten in the dimensionless domain: $0 \le u \le 1$, with $r = r_\infty + \Delta u$ (where $\Delta = r_\infty - r_{\text{fiber}}$), that is,

$$\frac{\partial C}{\partial t} = \frac{D_{\text{tissue}}}{\Delta^2}\left(\frac{\partial^2 C}{\partial u^2} - \frac{\phi}{(1-\phi u)}\frac{\partial C}{\partial u}\right) - S(C)$$

subject to

$$\frac{\partial C}{\partial u} = Bi_m(C^{\text{fiber}} - C) \qquad @\ u = 1$$
$$\frac{\partial C}{\partial u} = 0 \qquad @\ u = 0 \qquad \text{(A2)}$$

where

$$Bi_m = \frac{k_m\Delta}{D_{\text{tissue}}}$$

and

$$\phi = \frac{\Delta}{r_\infty}.$$

This equation can be solved by standard discretization techniques. For instance, following Finlayson (1980), orthogonal collocation discretization in symmetric polynomials will yield

$$\frac{\partial \underline{C}}{dt} = \frac{D_{tissue}}{\Delta^2}\underline{\underline{M}}\,\underline{C} + \underline{S(C)}$$

subject to

$$\sum_{j=1}^{N+1} A_{N+1,j}C_j = Bi_m(C^{\text{fiber}} - C_{N+1}), \qquad \text{(A3)}$$

where

$$\underline{C}^T = [C_1, C_2, \ldots, C_{N+1}]$$

and

$$M_{i,j} = \left[-\frac{\phi}{(1-\phi u_i)}A_{i,j} + B_{i,j}\right], \quad \text{with} \quad i,j = 1,2,\ldots,N+1,$$

where $A_{i,j}$ and $B_{i,j}$ are the collocation matrices, and N is the number of interior collocation points. The lumping approach can be illustrated by a one-term orthogonal collocation solution:

$$\frac{dC_1}{dt} = \frac{D_{\text{tissue}}}{\Delta^2}\left[M_{1,1} - \frac{M_{1,2}A_{2,1}}{A_{2,2} + Bi_m}\right]C_1 + \frac{D_{\text{tissue}}}{\Delta^2}\frac{M_{1,2}Bi_m}{A_{2,2} + Bi_m}C^{\text{fiber}} + S(C_1)$$

where

$$M_{i,j} = -\frac{\phi}{(1-\phi u_i)}A_{i,j} + B_{i,j} \qquad \text{(A4)}$$

and

$$\underline{\underline{A}} = \begin{bmatrix} -1.118 & 1.118 \\ -2.5 & 2.5 \end{bmatrix}, \quad \underline{\underline{B}} = \begin{bmatrix} -2.5 & 2.5 \\ -2.5 & 2.5 \end{bmatrix},$$

$$u_1 = 0.4772.$$

If the correction for cylindrical geometry is neglected (i.e., $\phi = \Delta/r_\infty \to 0$ for thin shells of tissue), the matrices become $M_{1,1} \approx B_{1,1}$ and $M_{1,2} \approx B_{1,2}$, and the one-term solution becomes

$$\frac{dC_1}{dt} = \frac{D_{\text{tissue}}}{\Delta^2} \frac{2.5Bi_m}{2.5 + Bi_m}(C^{\text{fiber}} - C_1) + S(C_1). \quad \text{(A5)}$$

This equation can be compared with a lumped-parameter model,

$$\frac{dC^{\text{tissue}}}{dt} = \frac{2k' r_{\text{fiber}}}{(r_\infty^2 - r_{\text{fiber}}^2)}(C^{\text{fiber}} - C^{\text{tissue}}) + S(C^{\text{tissue}})$$

$$= \frac{k'}{\Delta\left(1 + \dfrac{\Delta}{2r_{\text{fiber}}}\right)}(C^{\text{fiber}} - C^{\text{tissue}}) + S(C^{\text{tissue}}), \quad \text{(A6)}$$

which, for thin tissue shells, yields

$$\frac{\Delta}{k'} = \frac{\Delta^2}{D_{\text{tissue}}}\left(\frac{1}{Bi_m} + \frac{1}{2.5}\right)$$

or,

$$\frac{1}{k'} = \frac{1}{k_m} + \frac{\Delta}{2.5D_{\text{tissue}}} \Rightarrow P_t = \frac{D_{\text{tissue}}}{\delta} \quad \text{with, } \delta = \frac{\Delta}{2.5}. \quad \text{(A7)}$$

A similar problem has been addressed in the literature in lumping heat-transport resistances, where several different approaches have been presented, which could be extended to the problem formulated in this Appendix. These different lumping formulations differ in the approach toward the solution for the radial (temperature or concentration) profile. Beek and Singer (1951), for instance, assumed a parabolic radial profile; while Crider and Foss (1965) solved the linear problem in terms of Bessel functions. Their common result, however, is similar to the illustration just presented—that the lumped resistance takes on a general form $P_t = D_{\text{tissue}}/\delta$, with δ being a fraction of the thickness of the ring of tissue (i.e., $\Delta = r_\infty - r_{\text{fiber}}$). Since it can be shown that the solution in terms of a lumped-parameter model can be used to recover the radial profile (cf. Hlavacek and Votruba, 1977), and therefore the radial average value, a reasonable choice would be the distance at which the average value is observed. The calculation of r_∞ and δ are explained next.

Area of influence

To calculate the flow area (A_{flow}) used in Eqs. 5 and 6, we need to first determine the area of tissue around each fiber that is influenced by the insulin secreted from the fiber. This "area of influence," A_{tissue}, can be estimated using the following analysis.

Considering only radial diffusion, the mass conservation equation for insulin in the tissue surrounding the fiber will be given by (cf. Eq. A1):

$$\frac{\partial C_I^{\text{tissue}}}{\partial t} = D_{I,\text{tissue}} \nabla^2 C_I^{\text{tissue}}, \quad \text{(A8)}$$

where C_I^{tissue} is the insulin concentration in the tissue surrounding the fiber, and $D_{I,\text{tissue}}$ is the diffusion coefficient of insulin through tissue. If the tissue is assumed to be an infinite cylinder around the fiber, the initial and boundary conditions will assume the following form:

$$\begin{aligned} &C_I^{\text{tissue}} \to C_{I,\infty}^{\text{tissue}} && \text{for} && r \to \infty, && t > 0 \\ &C_I^{\text{tissue}} = C_I^{\text{fiber}} && @ && r = r_{\text{fiber}}, && t > 0 \\ &C_I^{\text{tissue}} = C_{I,\infty}^{\text{tissue}} && \forall && r, && t = 0, \end{aligned} \quad \text{(A9)}$$

where C_I^{fiber} is the maximum insulin concentration expected at the fiber surface, and $C_{I,\infty}^{\text{tissue}}$ is the initial concentration of insulin in the tissue. These equations can be rendered dimensionless by introducing the following definitions:

$$\theta = \frac{C_I^{\text{tissue}} - C_{I,\infty}^{\text{tissue}}}{C_I^{\text{fiber}} - C_{I,\infty}^{\text{tissue}}}, \quad \rho = \frac{r}{r_{\text{fiber}}} \quad \text{and} \quad \tau = \frac{tD_{I,\text{tissue}}}{r_{\text{fiber}}^2}. \quad \text{(A10)}$$

A closed-form solution for Eq. A9 can then be found as

$$\theta(\rho, \tau) = 1 + \frac{1}{2\pi}\int_0^\infty e^{-\xi^2\tau} F(\xi, \tau)\frac{d\xi}{\xi} \quad \text{(A11)}$$

where

$$F(\xi, \tau) = \frac{J_0(\rho\xi)Y_0(\xi) - J_0(\xi)Y_0(\rho\xi)}{J_0^2(\xi) + Y_0^2(\xi)}.$$

Alternatively, if the solution to the integral tends to diverge, a finite-difference approach could be used to find the concentration profile outside the fiber. The numerical approach was used here.

The dimensionless insulin profile was calculated as a function of time for three different fiber radii: 0.25, 0.5 and 1 mm. Since the objective was to calculate the tissue area influenced by the insulin within the time period over which the model is considered valid, the solutions were calculated for time = 25 min. The area of influence is defined by the radius at which the insulin radial transport is negligible. This is interpreted to be the radial position (r_∞) at which the insulin concentration drops to a small fraction (e.g., 10, 5 or 1%) of the insulin concentration at the fiber surface. The calculated values of r_∞ are shown in Table A1. The value of r_∞ used in

Table A1. Tissue Radii (r_∞) and Dimensionless Tissue Radii (ρ_∞) for Various Fiber Radii and Concentration Drop Criteria

r_{fiber}	$\theta = 0.1$		$\theta = 0.05$		$\theta = 0.01$	
(mm)	ρ_∞	r_∞ (mm)	ρ_∞	r_∞ (mm)	ρ_∞	r_∞ (mm)
0.25	4.80	1.20	5.64	1.41	7.32	1.83
0.5	2.85	1.42	3.30	1.65	4.10	2.05
1.0	2.00	2.00	2.25	2.25	2.62	2.62

Table A2. Lumping Distances (δ) for Different Concentration Criteria

	$\theta = 0.1$	$\theta = 0.05$	$\theta = 0.01$
δ, mm	0.485	0.578	0.726

our subsequent calculations (cf. Table 1) was that corresponding to a 95% concentration decrease.

The flow area of influence can then be readily calculated from r_∞ as

$$A_{tissue} = \pi(r_\infty^2 - r_{fiber}^2). \quad \text{(A12)}$$

The number of capillaries influenced by this fiber will be equal to the capillary density of the specific implantation site multiplied by the area of influence. The cross-sectional flow area, A_{flow}, can then be calculated from the sum of the individual capillary cross-sectional areas (Eq. 7).

Tissue permeability

In order to calculate the mass-transfer coefficient of Eq. 8, the permeability through the tissue surrounding the fiber is needed. This permeability is a function of the size of the region of tissue affected by the fiber, with the relationship given by Eq. A7. It is assumed that the lumping distance (i.e., δ in Eq. A7) can be chosen as the distance from the fiber at which the local insulin concentration equals the average value (Table A2). The diffusivity value, $D_{I,tissue}$, is given in Table 1.

Manuscript received Aug. 30, 1995, and revision received Feb. 21, 1996.